Acta Biomaterialia 33 (2016) 122–130

Contents lists available at ScienceDirect

Acta Biomaterialia

journal homepage: www.elsevier.com/locate/actabiomat

Full length article

Fabrication of conductive gelatin methacrylate–polyaniline hydrogels

Yibo Wu, Yong X. Chen, Jiahan Yan, David Quinn, Ping Dong, Stephen W. Sawyer, Pranav Soman *

Department of Biomedical and Chemical Engineering, Syracuse University, 900 S Crouse Ave, Syracuse, NY 13210, USA

ARTICLE INFO

Article history:
Received 3 August 2015
Received in revised form 11 January 2016
Accepted 23 January 2016
Available online 25 January 2016

Keywords:
Conductive hydrogels
Polyaniline
Gelatin methacrylate
Processing
Fabrication methods
Scaffolds

ABSTRACT

Hydrogels with inherently conductive properties have been recently developed for tissue engineering applications, to serve as bioactive scaffolds to electrically stimulate cells and modulate their function. In this work, we have used interfacial polymerization of aniline monomers within gelatin methacrylate (GelMA) to develop a conductive hybrid composite. We demonstrate that as compared to pure GelMA, GelMA–polyaniline (GelMA–Pani) composite has similar swelling properties and compressive modulus, comparable cell adhesion and spreading responses, and superior electrical properties. Additionally, we demonstrate that GelMA–Pani composite can be printed in complex user-defined geometries using digital projection stereolithography, and will be useful in developing next-generation bioelectrical interfaces.

Statement of Significance

We report the fabrication of a conductive hydrogel using naturally-derived gelatin methyacrylate (GelMA) and inherently conductive polyaniline (Pani). This work is significant, as GelMA-Pani composite has superior electrical properties as compared to pure Gelma, all the while maintaining biomimetic physical and biocompatible properties. Moreover, the ability to fabricate conductive-GelMA in complex user-defined micro-geometries, address the significant processing challenges associated with all inherently conductive polymers including Pani. The methodology described in this work can be extended to several conductive polymers and hydrogels, to develop new biocompatible electrically active interfaces.

1. Introduction

Motivated by the goal of repairing and regenerating diseased tissue, the past decades have seen the emergence and growth of the field of tissue engineering in which 3D scaffolds are developed in combination with cells and biomolecules [1–7]. Hydrogels which form 3D cross-linked hydrated fibers, have emerged as the ideal material for developing scaffolds because of its similarity to the natural extracellular matrix, as well as their ability to tune mechanical and biochemical cues [8–14]. However, hydrogels are typically non-conductive, which limit their application in modulated cell function for excitable cell types such as nerve, and muscle cells, as well as non-excitable cells which also possess a negative intercellular voltage [15–20]. An electroconductive hydrogel would give researchers the ability to provide an electrical cue to living cells using an extracellular matrix (ECM)-like environment, towards understanding the often unexplored role of electrical energy in modulating cellular responses [21–30]. Thus far, the approaches to develop conductive hydrogels can be broadly classified into (a) hydrogels mixed with conductive elements, and (b) hydrogels mixed with inherently conductive polymers (ICPs) [21,24,31].

One approach involves doping hydrogels with conductive particles, including nanofibers/nanowires [32,33], graphene [34,35], metallic nanoparticles [36,37], or carbon nanotubes (CNTs) [22,36,38–40] within its matrix. In another approach, inherently conductive polymers (ICPs) such as poly(pyrrole) (PPy), poly(3,4-ethylenedioxythiophene) (PEDOT) and polyaniline (Pani), are integrated or infused within hydrogel matrix such as polyethylene glycol and polyacrylamide [21,24,41–44]. As compared to other ICPs, polyaniline (Pani) is easy to synthesize and has acceptable environmental stability [42,45], and has been shown to be compatible with specific cell types [46] however its use in developing 3D scaffolds for tissue engineering is limited because of multiple reasons. Pani has low processability, low flexibility, and is not biodegradable and has been shown to be cytotoxic to several cell lines (probably due to leaching of low-molecular by-products and

* Corresponding author.
E-mail address: psoman@syr.edu (P. Soman).

http://dx.doi.org/10.1016/j.actbio.2016.01.036
1742-7061/

residual acid) [46,47]. Typically a biological adhesive coating is applied to Pani to improve its cell adhesion properties [46,48].

To address these challenges, Pani has been integrated with synthetic and naturally-derived hydrogels to develop conductive-hydrogels with sufficient biocompatibility, as well as cell adhesion [24,49,50]. However, the low processability of Pani (the ability of a polymer to be processed into functional devices and complex user-defined geometries), has not been sufficiently addressed. The primary reason of Pani's poor processability is its low solubility in organic solvent as well as its brittle characteristic due to the presence of rigid π-conjugated bonds [51]. Although 2D thin micrometer-resolution Pani films have been developed using a variety of methods such as inkjet printing, casting, self-assembly, electrospinning etc., [23,52–57], processing Pani into 3D complex geometries remain a challenge.

In our previous work, interfacial polymerization of aniline monomers within a synthetic hydrogel (polyethylene glycol diacrylate – Pegda), was used to develop Pani–Pegda composite [58], however its utility for serving as a cell-scaffold was found to be limited, as synthetic non-biodegradable Pegda lack naturally-occurring bioactive epitopes, and incorporating biofunctional groups after polymerization of Pani–Pegda was found to be challenging. In this work, we use gelatin methacrylate (GelMA) hydrogel, which possesses naturally-occurring distribution and variety of biofunctional groups which support cell adhesion, to synthesize a GelMA–Pani composite. Since GelMA maintains a robust structure for about 4 weeks, and completely degrades in about 6–8 weeks post cell-seeding, GelMA–Pani composite can potentially be an attractive platform to investigate cellular responses of electrical cues.

2. Materials and methods

2.1. Synthesis of GelMA–Pani hydrogel

Gelatin methacrylate (GelMA) was synthesized by addition of methacrylate groups to porcine gelatin using a previously optimized protocol [59–62]. GelMA precursor solution was prepared by mixing GelMA dissolved in DI water (10%; w/v) with 0.25% (w/v) Irgacure 2959 photoinitiator. GelMA precursor solution was injected between two glass slides, Teflon spacers and a rectangular mold and subsequently shone with UV light (Omnicure S2000 UV lamp, Lumen Dynamics, Quebec, Canada) for 10 min, to prepare a solid crosslinked GelMA hydrogel sheet (thickness = 1.62 mm). A circular punch (diameter = 16 mm) was used to punch out circular disc-shaped GelMA samples. Samples were stored in DI water for 24hrs to remove any uncrosslinked monomers and unreacted photoinitiator. GelMA disc-shaped samples were immersed in 1 M HCl solution containing 0.04, 0.08 and 0.16 M ammonium persulfate (APS) (P1, P2 and P3 respectively) for 4 hours (Fig. 1), and then immersed in hexane solution containing 0.16 M aniline for another 4 hours. Dark green GelMA–Pani samples were purified in DI water for 3 days and 1 M HCl solution for another 2 days to remove any residual unreacted aniline and by-products. The control samples include pure GelMA (C1) with no processing, and GelMA immersed in HCl but not in aniline solution (C2).

2.2. Fourier Transform infrared spectroscopy (FTIR)

FTIR spectra of the GelMA (C1), GelMA–Pani (P2), and central slices from GelMA–Pani (P2) hydrogel samples were recorded using Spectrum One FTIR Spectrometer from PerkinElmer Instrument. Samples were kept intact or sliced, before freezing below −80 °C overnight and freeze-dried for 24 h. Samples were placed in the rack of the FTIR machine. The Spectrum One computer interface software was used to record their FTIR spectra.

2.3. Swelling ratio

GelMA and GelMA–Pani hydrogel samples (5 mm in diameter and 1.62 mm in thickness) were incubated in DI water for 3 days and dried for 48 hours at room temperature. The mass swelling ratio was measured by comparing the hydrated weight (W_w) over the dehydrated weight (W_i) using equation: mass swelling ratio (%) = $((W_w - W_i)/W_w) \times 100\%$.

2.4. Compressive modulus

Compressive modulus of pure GelMA and GelMA–Pani composite (5 mm in diameter and 1.62 mm in thickness) were evaluated using a dynamic mechanical analysis (DMA) machine (Q800, TA Instruments, Inc.). Samples of different aniline/APS ratios were incubated in phosphate buffer saline (PBS) at 37 °C for 48 h. Samples were loaded under compression clamp and tested for controlled strain percentage (ramping from 0 to 40%) with preloaded force of 0.01 N and displacement of 10 μm. Slope of stress–strain curve from 0 to 10% strain was used to determine compressive modulus.

2.5. Scanning electron microscopy (SEM)

GelMA and GelMA–Pani samples were frozen (−80 °C), freeze dried for 24 h, mounted on an aluminum SEM stub with double-sided carbon tape, sputter coated with gold for 45 s, and images were taken at 5 kV (Joel 5600 SEM, Japan).

2.6. Contact angle

The water contact angle measurements of GelMA and GelMA–Pani samples were performed using the VCA Optima (AST Products, Inc.). A drop of DI water (0.75 ml) was placed on the sample and a digital camera was used to record images of water menisci. For each type of sample, contact angle was measured for 4 independent samples.

2.7. Cell culture and immune labeling

C3H/10T1/2 murine mesenchymal progenitor cells (10T1/2s), were cultured in BME supplemented with 10% fetal bovine serum, 1% Glutamax, 1% Penstrep, and were maintained in a 37 °C incubator with 5% CO_2. Cells were passaged using standard cell culture protocols using 0.25% trypsin–EDTA and were used within passage number 15. Cells were harvested, and seeded on GelMA and GelMA–Pani samples at a concentration of 5×10^5 cells/ml, with media changed 1 day after seeding, and refreshed every other day. Cells were fixed on day 5 using 4% paraformaldehyde (Invitrogen, Carlsbad, CA) overnight at room temperature, permeabilized with 0.1% Triton X-100 (Sigma-Aldrich) in PBS with 1% bovine serum album (BSA, Hyclone) for 30 min. F-actin was labeled with Alexa 488 or Alexa 647 (Invitrogen, Carlsbad, CA) (dilution 1:40) while nucleus was labeled using Hoechst 33258 DNA dye (Invitrogen, Carlsbad, CA) (dilution 1:1000) for 30 min. Fluorescence microscopy and confocal fluorescence imaging was performed using Leica DMI4000B and Zeiss LSM 710 respectively, and image analysis was performed using ImageJ. To evaluate cellular viability, a live/dead assay (Invitrogen, Carlsbad, CA) was used to stain cells using calcein-AM/ethidium homodimer using $n \geqslant 5$ independent samples and visualized using fluorescence microscopy. Dead cells appear as Red, while live cells appear as green, and viability was

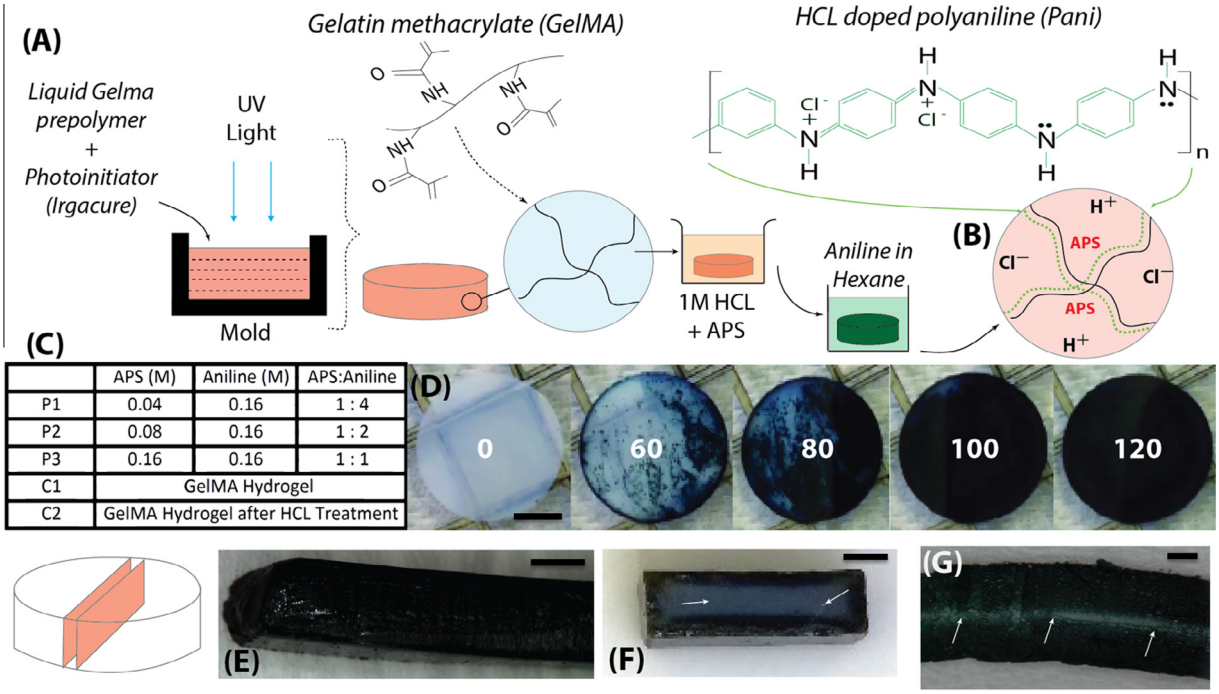

	APS (M)	Aniline (M)	APS:Aniline
P1	0.04	0.16	1 : 4
P2	0.08	0.16	1 : 2
P3	0.16	0.16	1 : 1
C1	GelMA Hydrogel		
C2	GelMA Hydrogel after HCL Treatment		

Fig. 1. Synthesis and formation of gelatin methacrylate-polyaniline (GelMA–Pani) conductive hydrogel using interfacial in situ polymerization method: (A) GelMA hydrogel is crosslinked within a mold using UV light. (B) Crosslinked GelMA sample immersed in HCl solution containing ammonium persulfate (APS), is transferred to a solution mixing hexane with aniline, resulting in Pani formation with GelMA matrix. (C) Table lists various ratios of APS to aniline (P1, P2, and P3) as well as the control samples (C1 and C2) used in this work. (D) Semi-transparent GelMA hydrogel gradually becomes dark green (black) color as a function of time (in minutes) with the formation of emeraldine salt Pani polymers. Scale bar: 5 mm (Control samples: C1 is pure GelMA without any processing; C2 is GelMA sample immersed in HCl but not in aniline solution). (E–G) Images depicting sliced sections of GelMA–Pani samples with different sample thicknesses and incubation time in aniline–hexane solution. Sample thickness (1.62 mm) with 4 h of incubation time has dark green (black) color (E), while samples (1.62 mm) with 5 min of incubation time has black color only on the outer edges (F), and samples (3 mm) with 4hrs of incubation time has a faint-green region in the center. (White arrows indicate partially crosslinking Pani) Scale bar: 1 mm. (For interpretation of the references to colour in this figure legend, the reader is referred to the web version of this article.)

calculated as a percentage of live cells as compared to total number of cells.

2.8. Electrochemical impedance spectroscopy (EIS)

The electrical properties of GelMA–Pani composite, GelMA control and Titanium metal control samples were tested using a three electrode system at a frequency range of 0.02–20 k Hz and an AC perturbation of 10 mV. Disk-shaped GelMA–pani samples were placed onto a Titanium electrode to serve as the working electrode which was assembled into an electrochemical cell with a circular-hole (diameter 8 mm) on top of the hydrogel. Ag/AgCl, carbon electrodes and 1 M H_2SO_4 solution were used as the reference electrode, counter electrode and electrolyte respectively. Solartron Analytical 1280Z working station was used to drive electrochemical impedance spectroscopy test. Data was collected by *Z* plot and analyzed by Z view software.

2.9. Direct current resistance measurement

A direct current resistance measurement system was developed. This system is composed of a Data Acquisition (DAQ) system and a planar gold measurement chip (Figs. 3E, F and SI-B). The DAQ utilized a single ended analog input of a National Instruments USB 6211Data acquisition system. The analog input channel has a 10 GΩ input impedance with 100 pF capacitance to ground and a sensitivity of 91.6 μV. A 100 kΩ resistor is placed in series with the sensing electrodes (Fig. 3E) and a constant voltage (5.0 V) was applied across the series resistor and the ground electrode of the chip. The DAQ measures the voltage drop between the electrodes (a function of the conductivity of the hydrogel sample) at given intervals and tracks the changes in the effective resistance of hydrogel sample over time. This system records a voltage value 20 times per second and a running average of 5 samples is utilized to smooth out noise in the measurement system. The measurement chip is configured with planar electrodes that are adhered to an FR-4 printed circuit board substrate (Fig. 3E and F). FR-4 is a glass fiber laminate materiel that is commonly used for electronic circuit boards and exhibits very low water absorption. The chip electrodes are constructed of etched copper 0.017 mm thick, plated with nickel and then plated with a gold surface. The exposed electrodes are connected to wires via copper traces that run underneath electrically insulating film to pads that have wires soldered to them that connect to the DAQ analog input channel. The Electrode pads are 3 mm × 1 mm separated by a 2 mm space between the electrodes. (Refer to SI-B for the full chip design with 8 electrode pairs).

2.10. Methacrylation of glass coverslips

Round glass coverslips (12 mm Dia, Chemglass Life Sciences, Vineland, NJ) were agitated in Piranha solution (sulfuric acid: hydrogen peroxide = 7:3 ratio) for 5 min, washed in DI water 3× (5 min each time), and washed in 100% ethanol (Fisher Scientific, Pittsburgh, PA) and dried with nitrogen. Dried glass coverslips were functionalized in a bath containing 85 mM 3-(Trimethoxysilyl)propyl methacrylate (Fluka, St. Louis, MO) in ethanol with acetic acid (pH 4.5) with overnight rocking at room temperature. Modified coverslips were washed with ethanol (5×, 5 min each wash cycle), dried with nitrogen, and baked in oven for 1 h.

2.11. Digital projection stereolithography

The main components of the fabrication system are a UV light source (EXFO Omnicure S2000, wavelength range 320–500 nm,

Quebec, QC, Canada), a digital light processing (DLP) chip (Discovery 4000, Texas Instrument, TX), and computer controlled stages (Newport 426/433 series). The DLP is an electronic board embedded with an array of 1920 × 1080 square mirrors, which convert user-defined bitmap files into virtual masks or projections, selectively switching mirrors into either the ON state or the OFF state. The mirrors in the ON state project digital images onto the liquid prepolymer solution. Areas illuminated by UV light crosslink, while the dark regions remain in liquid uncrosslinked state, thereby selectively polymerizing GelMA into hexagonal cellular geometry. These patterns were irradiated for 10 s at a projected UV intensity of ~25 mW cm^{-2}.

3. Results

3.1. Synthesis of GelMA–Pani

In this work, disc shaped GelMA was crosslinked using UV light, and subsequently interfacial in situ polymerization method was used to polymerize aniline monomers within the hydrogel matrix, to form the GelMA–Pani hybrid matrix. Briefly, three steps are involved in the synthesis of GelMA–Pani hydrogel composite. In step 1, UV light exposure generates free radicals to activate functional monomers to form covalent bonds and develop a semi-transparent crosslinked GelMA gel (Fig. 1A). In step2, GelMA samples were immersed in a solution of 1 M hydrochloric acid (HCl) containing ammonium persulfate (APS) (Fig. 1B), making GelMA matrix acidic, which helps in selective polymerization of aniline monomers in the next step. Finally in step 3, acidic GelMA sample is transferred into hexane (an organic solvent) containing aniline monomer, resulting in formation of emeraldine salt (conductive) form of Pani. Semi-transparent GelMA hydrogel becomes opaque with the formation of the Pani (dark-green color) (Fig. 1D). The GelMA–Pani hydrogel composite is thoroughly purified by DI water for 3 days and HCl for another 2 days, to allow any residual APS, low molecular weight Pani and other by-products to leach out. Selective polymerization of Pani prevents leaching out of newly synthesized Pani, as no color change is observed when a GelMA–Pani composite is immersed in a clear solution of DI water. In this work, the ratio of APS to aniline was varied by only increasing the concentration of APS, such that APS concentration never exceed aniline concentration to prevent over-oxidation of Pani, thus maintaining the conductive half-oxidized Pani (emeraldine salt) state. (Fig. 1C) Two control samples were also included (C1-pure GelMA; C2-GelMA sample undergoing HCl treatment, but not immersed in aniline solution). To ensure that Pani has crosslinked throughout the GelMA matrix, two control experiments were performed. First, the sample size was kept constant (1.62 mm thickness and 16 mm diameter), while the incubation time in aniline–hexane solution was decreased to 5 min, and compared to the incubation time used in this work (4 h). Both samples were sliced from the central portion of the disc-shaped sample. We found that with increase in incubation times, the transparent-white GelMA changes from white color to green to dark green/black (Fig. 1E). Dark green/black color typically represents the formation of Pani within GelMA matrix. At decreased time of 5 min incubation, green color is observed only on the outer layer of the cross-sectional slice, cut from the disc-shaped sample (White arrows in Fig. 1F). Second, the sample size was changed to 3 mm thickness as compared to 1.62 mm (used in this work), while maintain the 4 h aniline incubation time (used in this work). A thin light-green strip is observed in the center of the central slice of GelMA–Pani, indicating that partial-crosslinking of Pani within the GelMA matrix (White arrows in Fig. 1G). These two experiments demonstrate that scale/-size as well as incubation times, have significant influence on Pani crosslinking within GelMA, and these parameters have to be optimized to obtain uniform Pani–GelMA samples. For the size and incubation times used in this work, we find that Pani has integrated throughout the bulk GelMA matrix.

3.2. Characterization of GelMA–Pani composite

The presence of Pani within GelMA matrix was verified using FTIR. FTIR spectra taken from intact GelMA, intact GelMA–Pani samples, and a central-slice of the GelMA–Pani sample show the aniline peak (around 1140) in both intact GelMA–Pani samples, indicates the Pani has reacted throughout the sample although the peak of the sliced sample is smaller as compared to the intact sample, possibly because of the reduced thickness of the sliced sample. For P2 sample, we observed a distinct change in peak at 1141 which represent the in-plane bending of C–H in aromatic moieties, indicating emeraldine (conductive) salt form of Pani (Fig. 2A). Scanning electron microscope (SEM) images demonstrate filling up of the porous GelMA microstructure with Pani, resulting in smaller pore-size (Fig. 2D and E). Mass swelling ratio of GelMA and GelMA–Pani samples (3D disc of 16 mm diameter and 1.62 mm thickness) at various stages of processing (C1 and C2), with various aniline ratios (P1, P2 and P3) were characterized (Fig. 2B). Results demonstrate no significant differences between GelMA–pani and GelMA samples although we do observe a slight increase in swelling ratio for C2 when compared to C1, which can be attributed to the breaking of some porous structure resulting in increased pore size, probably caused by the hydrolysis of HCl. A decrease of swelling ratio for P1, P2 and P3 as compared to C2 was also noted, attributed to the infusion of Pani within GelMA matrix, thereby decreasing the pore size, also indicated by the SEM images. Since it is well recognized that compressive modulus (stiffness) significant influences cell-materials interactions, compressive moduli for GelMA controls (C1, C2) and GelMA–Pani composites were characterized using Dynamic Mechanical Analyzer (Fig. 2C). Compressive modulus of GelMA control without any treatment (C1) was found to have the stiffness value of 12.62 ± 0.65 kPa. With HCl treatment (C2), the modulus decreased to a value of 12.34 ± 0.48 kPa, probably due to HCl-enabled damage of the internal microporous structure of GelMA hydrogel. Modulus increases with increases amount of Pani, likely due to incorporation of Pani within GelMA hydrogel network. The net change in modulus between pure GelMA (~12.3 kPa) and GelMA–Pani (13.7–15.2 kPa) is a few kPa, indicating that interfacial polymerization process did not significantly alter the modulus, and still lies within the physiological range of stiffness of various cell types.[1] To evaluate the biocompatibility for the GelMA–Pani composite, C3H/10T1/2 murine mesenchymal progenitor cells (10T1/2s) were seeded and cell viability was evaluated on day 5 post-seeding. The green fluorescent dye calcein indicated viable cells, and red nuclei showed damaged and dead cells with the membrane-dye Eth-D1 (Fig. 2G and H). The samples exhibit cell viability similar to a control experiment on pure GelMA sample. Contact angle of GelMA–Pani (P2) is lower as compared to control GelMA (C1), however the difference is not significant (Fig. 2F). As a result, we anticipate that small differences in hydrophilicity would not significantly contribute to the observed cell responses. The morphology of seeded cells were evaluated by staining samples with actin and nuclei. As compared to GelMA control (Fig. 2I), which demonstrates abundant cell spreading, GelMA–Pani (P2) demonstrated less moderate to less cell spreading, possibly because of the presence of Pani. (Fig. 2J).

3.3. Electrical characterization of GelMA–PANI

Electrical properties of GelMA and GelMA–Pani samples were evaluated using Electrochemical Impedance Spectroscopy (EIS) and a custom-made resistance-test-chip.

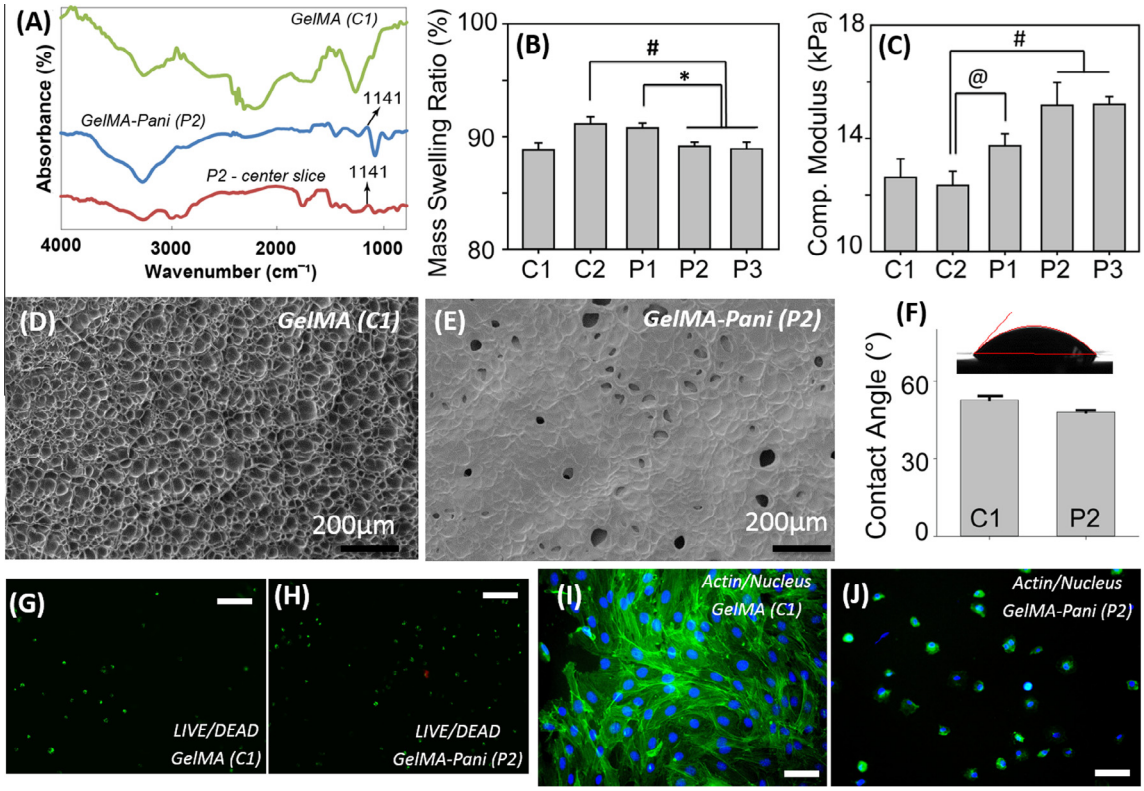

Fig. 2. Material characterizations and biocompatibility of GelMA and GelMA–Pani samples: (A) FTIR curve of intact GelMA–Pani and sliced section obtained from center slice of GelMA–Pani sample shows a distinct peak at 1141 cm^{-1}, (B) Mass swelling ratios and (C) compressive moduli of various samples, (D and E) SEM pictures of GelMA and GelMA–Pani showing difference in pore morphology, (F) Contact angle analysis, (G and H) Representative images of viability of 10T1/2 cells seeded on GelMA and GelMA–Pani samples as assessed via calcein–AM (green)/ethidium homodimer (red) assay 5 days post-seeding. (I and J) Morphology of 10T1/2 cells on GelMA control and GelMA–Pani samples as depicted by F-actin (green) and nuclei (blue) 5 days post-seeding. ($^{\#}p < 0.001$; $^{*}p < 0.01$; $^{@}p < 0.05$; NS: not significant) Scale bar G and H: 100 µm; Scale bar I and J: 10 µm. (For interpretation of the references to colour in this figure legend, the reader is referred to the web version of this article.)

3.3.1. Electrochemical impedance spectroscopy (EIS)

In EIS, a small sinusoidal AC voltage perturbation was applied to the samples of interest (Titanium metal control-Ti, GelMA control-C1 and GelMA–Pani composite-P2) around its open circuit potential (OCP) over a range of frequencies (0.02–20 kHz) with an amplitude of 10 mV. Results were plotted in the form of Nyquist and Bode Plot (Fig. 3A–C), and data was fitted with a standard Randles cell (RC) equivalent circuit model (Inset in Fig. 3B). ZView software was used to obtain values of constant phase element (CPE, which replaces the ideal capacitance), the uncompensated solution resistance (R_s) and the polarization resistance (R_p). CPE represents the reaction step when electrons/ions build up on a surface, while R_p indicates the transport of charge through materials or interfaces. Compared to C1, P2 exhibited lower impedance, indicated by a smaller diameter of the partial-semi-circle (Fig. 3A). The magnitude of impedance is also affected by the frequency value as depicted by Bode plots (Fig. 3B) with impedance magnitude plotted against range of frequencies. Both GelMA and GelMA–Pani samples exhibit low impedance at high frequencies (1 kHz) due to capacitive currents, however at physiologically-relevant low frequencies, the impedance of GelMA–Pani (2.9 ± 0.3 kΩ) is significantly lower than pure GelMA sample (6.9 ± 0.7 kΩ) (Figs. 3D and SI-B) likely because of resistive currents through the conjugated Pani backbone crosslinked within GelMA matrix. In the plot of phase angle verses frequency, both GelMA and GelMA–Pani show only one peak, while with Ti control, we observe two distinct peaks. The resistance (R_p) of pure GelMA (C1) (~4.9 kΩ) is smaller than the GelMA–Pani (P2) (~16.3 kΩ (SI-B) while the capacitance of C1 (~0.03F) is higher than P2 (~0.01F), indicating the conductive GelMA–Pani interface represented by the capacitive element in Randles circuit.

3.3.2. Resistance measurement chip

In addition to EIS, a custom-made resistance testing chip (Fig. 3E–H) was used to directly record the real-time resistance change for Ti control, GelMA (C1) and GelMA–Pani (P2) samples. Test samples were presses against the parallel electrodes, and the changes in resistance were recorded for 10 min, using Labview software. As expected, the resistance did not change for the Titanium metal control sample, and remained at a low value of ~7 Ω (Fig. 4H). Both GelMA (C1) and GelMA–Pani (P2) demonstrated an initial increase of resistance before reaching saturation at ~500 and ~200 s respectively (Fig. 4G and SI-C), with a resistance of C1 (508.60 ± 6.84 Ω), and P2 (165.56 ± 5.97 Ω), calculated by averaging the last five data points, and demonstrates a significant decrease in conductivity for the Pani-doped GelMA as compared to pure GelMA.

3.4. Printing of GelMA–Pani using micro-stereolithography apparatus (µSLA)

Conductive polymers, including Pani, are typically processes in form of thin films or using molding approaches. In this work, we demonstrate that GelMA–Pani composites with user-defined patterns can be fabricated. The µSLA utilizes a digital micro-mirror projection (DLP) array (Texas Instruments) to develop virtual or digital masks, and selectively switch mirrors into either the ON state or the OFF state (Fig. 4A). The mirrors in their ON state reflect UV light beams into the focusing lens, and project them onto a GelMA prepolymer solution (a mixture of 10% GelMA and 0.1% photoinitiator), while the mirrors in OFF state diverts the UV light away from the solution. A hexagonal cellular pattern was designed and uploaded onto the DLP chip (Fig. 4A). UV light modulated by

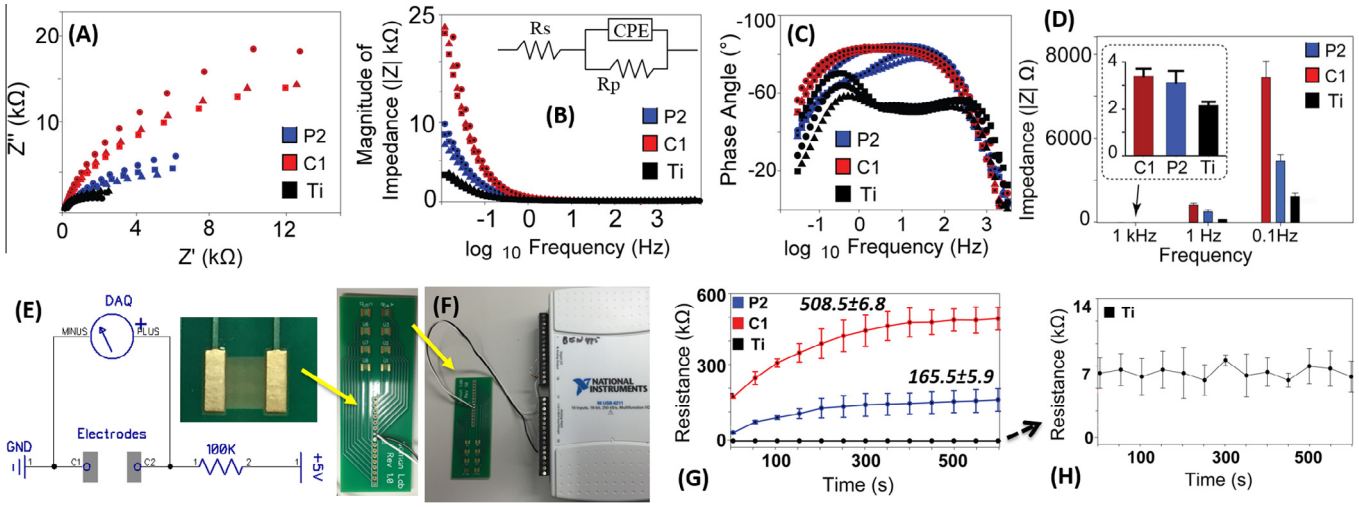

Fig. 3. Electrical characterizations of GelMA–Pani composites: (A–D) Electrochemical impedance spectroscopy (EIS) was used to obtain Nyquist and Bode plots for C1, P2 and Ti (C1 = red; P2 = blue and Ti = black) for a range of frequencies. Data was fitted to Randles equivalent circuit, and values of capacitance element (CPE), R_s, the solution resistance and R_p, polarization resistance were obtained. GelMA–Pani (P2) sample show lower resistance to electron transfer as indicated by the decrease in the diameter of the semi-circular curve. The magnitude of P2 is significantly lower that control (C1-pure GelMA) especially at physiologically-relevant lower frequencies. (E–H) A custom-made resistance measurement chip was fabricated, and used to test variations in bulk resistance of standard disc-shaped samples over time. (E and F) Schematic of the logic electric circuit and images of the actual chip. (G) Change of resistance of P2, C1 and Ti samples as a function of time, demonstrates a significantly higher resistance value of pure GelMA (C1) as compared to GelMA–Pani (P2) sample. As expected, the resistance of Titanium (Ti) is much less, and is plotted separately in H. (For interpretation of the references to colour in this figure legend, the reader is referred to the web version of this article.)

the virtual mask in the form of hexagonal pattern, was focuses onto the GelMA prepolymer solution, to generate free radicals, and crosslink a semi-transparent crosslinked GelMA hexagonal pattern, similar to step 1 in Fig. 1A (Fig. 4B). A modified glass coverslip was used for this process, to ensure good adhesion between crosslinking GelMA and glass substrate, primarily for ease in handling during cell seeding and imaging steps. The samples underwent the interfacial in situ polymerization process to allow diffusion of aniline monomers within the sample, and crosslink within the GelMA network, to form opaque dark-green GelMA–Pani composite with hexagonal geometry (Fig. 4C). APS to aniline ratio was set to be 1:2 (P2). 10T1/2s cells were seeded on control GelMA (C1) and GelMA–Pani composite (P2), and morphology of adhered cells were evaluated by staining the samples for actin and nuclei (Fig. 4D–F). In control GelMA (C1) samples, cell exclusively spread and adhere to GelMA, while cells adhere the GelMA–Pani as well as the space between the structures.

4. Discussion

In vivo physical, biochemical and electrical stimuli play a vital role in regulating cellular function and tissue growth. With the goal of understanding and utilizing in vivo stimuli for modulating cellular function, new platforms continue to be developed, and remains an intensive area of research [15–31]. With the realization that electrical cues play an essential role in controlling cell function, such as morphology, proliferation and migration, researchers have continued to develop new biomimetic electroconductive platforms and scaffolds using advances in polymer chemistry and microfabrication techniques. Recently, conductive hydrogels have been developed to provide stimulus or respond to electrical cues to or from living cells, by combining hydrogels with conductive particles, both inorganic particles as well as various ICPs [63]. However fabrication of conductive hydrogels into complex geometries remains a challenging task.

In this work, we developed a novel electroconductive hydrogel using gelatin methacrylate (GelMA) and inherently conductive polyaniline polymer using interfacial polymerization, a recent chemical route of synthesizing conductive polymeric structures [64–66]. In interfacial polymerization, the monomers of conductive polymers (dissolved in organic solvent) are mixed with oxidants (dissolved in water), to generate conducting polymers at the organic-solvent/water interface (Fig. 1). This approach provides marked improvement over the conventional approach of forming conductive hydrogels by mixing conductive particles within hydrogel matrix, which typically results in poorly integrated composite [25,67,68]. GelMA is a good choice for this work, as it is a denatured form of collagen (the most abundant protein found in the body) and has been shown to maintain its structural integrity for more than 4 weeks, before onset of degradation. Crosslinked GelMA is a mesh-like hydrated structures with sufficient space for diffusion of another biochemical species (aniline monomers in this case). Polymerization occurs at the interface between the hydrophilic GelMA hydrogel and the hydrophobic hexane solution. Since conductive Pani synthesized in acidic environment is in its hydrophilic emeraldine salt state, it spontaneously and exclusively migrates into the hydrophilic hydrogel matrix and is confined within the GelMA matrix. Moreover, selectivity of Pani polymerization around hydrogel network chains maintains diffusion of newly synthesizes Pani and APS throughout the GelMA sample, resulting in uniform conductive properties of the sample, as compared to other processes where Pani polymerization typically blocks the surface micropores and prevents polymerization in the interior of the 3D bulk composite. However, the exact mechanism of Pani crosslinking within GelMA matrix is not known, and future work has to be carried out to understand how Pani-crosslinking relates to solvent type, molecular dispersions, relative amounts and pore-sizes.

Based on the swelling, compression and biocompatibility testing, the GelMA–Pani composites are similar in properties to the pure biomimetic GelMA hydrogels, and therefore closer to the properties of in vivo extracellular matrix (Fig. 2). This means that although more electro-conductive as compared to other biomaterials, GelMA–Pani composite would elicit cellular responses similar to pure GelMA and other biomaterials of similar properties, and would serve as a suitable conductive scaffold. This is an advantage

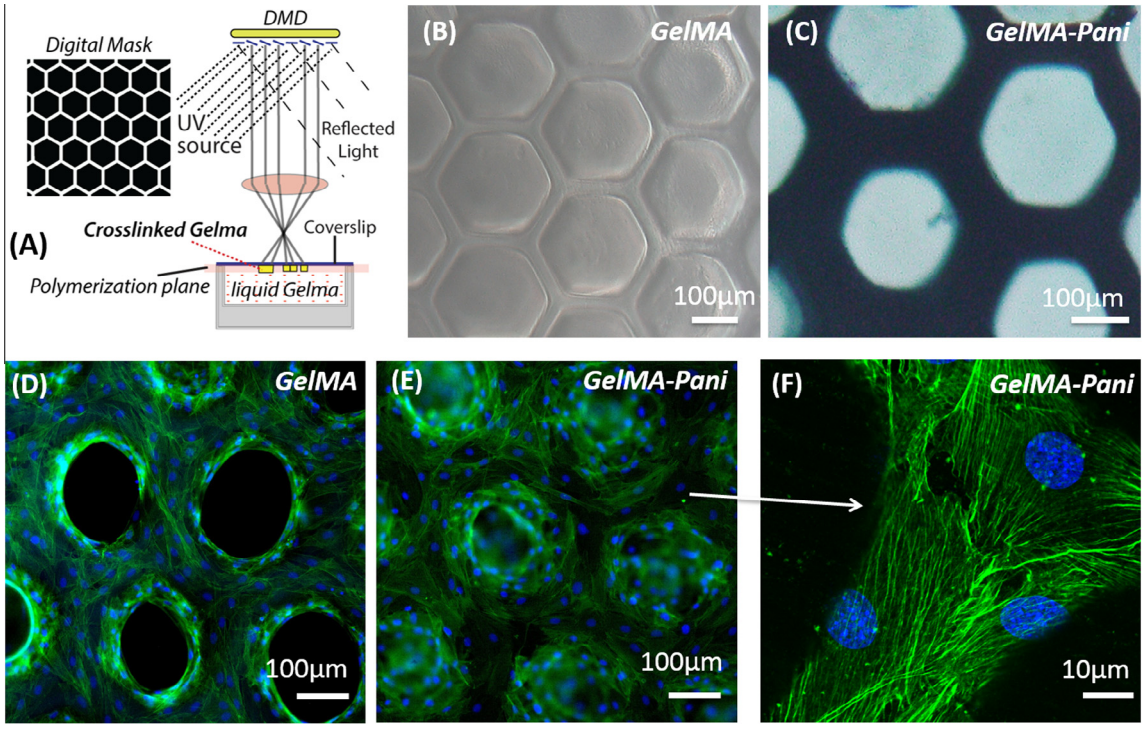

Fig. 4. Fabrication of GelMA–Pani using user-defined hexagonal geometry: (A) Schematic of digital projection microstereolithography: Liquid GelMA precursor solution is placed in a chamber covered by a methacrylated glass coverslip. Computer aided design (CAD)-based digital mask with hexagonal pattern is used to modulate UV light, and selectively polymerize GelMA. (B and C) Brightfield images of GelMA (semi-transparent) and GelMA–Pani (dark-green) with hexagonal geometry. (D–F) Fluorescence and confocal images of GelMA and GelMA–Pani samples seeded with 10T1/2 cells, and labelled for actin (green) and nucleus (blue). (For interpretation of the references to colour in this figure legend, the reader is referred to the web version of this article.)

as compared to doping-based approaches of fabricating conductive hydrogels, where conductive particles added to the hydrogel network result in significant increase of their mechanical properties.

Cell adhesion and viability on GelMA and GelMA–Pani composites, (Figs. 2G–I and 4D–F), demonstrate similar responses. This result demonstrates the presence of bioactive sites on GelMA–Pani composite, even after going through harsh processing conditions (organic solvent and HCl acid). Please note that GelMA–Pani samples were not incubated with any adhesive protein before seeding cells, a common cell-seeding protocol to encourage adhesion of cells to biomaterials.

Nyquist diagrams, with imaginary ($-Z''$) verses real (Z') components of impedance, were plotted from time constants derived from Randles equivalent circuit (capacitive element-C, solution resistance $-R_s$, and polarization resistance $-R_p$) (Fig. 3). From SI section, R_p (resistance to transport of charge through a material) for GelMA–Pani is higher (16.3 kΩ) as compared to pure GelMA (4.9 kΩ), however the combined/total impedance of pure GelMA is higher, primarily because capacitance, C (reaction step of building charge on a surface) is higher for pure GelMA (0.032F) as compared to GelMA–Pani (0.014F). This implies that the transport of charge through pure GelMA is more efficient as compare to GelMA–Pani, probably because of free diffusion of ions, which gets disrupted because of Pani crosslinking. However, Pani crosslinking decreases the capacitance of pure GelMA, by allowing easier charging of interfaces between two internal segments. Bode diagrams in Fig. 3B, with impedance magnitude plotted against range of frequencies, depict that at physiologically relevant lower frequencies, GelMA–Pani (P2) has much lower impedance as compared to pure GelMA (C1). Direct current resistance measurements of the samples revealed a characteristic change in resistance versus time, with lower overall resistance values for GelMA–Pani samples as compared to pure GelMA. Lastly, fabrication of GelMA–Pani in complex user-defined geometries was demonstrated by μSLA approach, which can be potentially extended to variety of complex geometries, conductive polymers, and photosensitive biopolymers. One limitation of this approach with respect to scalability is the overall projection area (XY) during single UV exposure, which is typically around 4 mm × 4 mm. Although larger sizes can be printed by step projection printing, a method where the stage is translated along XY in a stepwise manner, this results in mismatched interfaces between two adjacent stitched sections.

5. Conclusions

In this work, we used interfacial in situ polymerization method to develop a novel biocompatible electroconductive GelMA–Pani composite. FTIR and SEM results indicate the existence of emeraldine salt (conductive) Pani within GelMA matrix. GelMA–Pani can be fabricated using standard fabrication approaches such as UV photocrosslinking, and show similar mechanical, swelling, and cell adhesion properties as compared to biomimetic GelMA. Results demonstrate improved electrical properties as compared to pure GelMA using EIS measurements and custom-developed resistance-chip. We also demonstrated the fabrication of GelMA–Pani with defined microarchitecture using digital stereolithography. This approach has the potential to be extended to a wide variety of photosensitive hydrogels as well as other biopolymers and cells, to drive the development of new bioelectrical interfaces for several biomedical applications.

Author contribution

Y.W. synthesized samples, carried out electrical testing, and analyzed data; Y.X.C. performed DMA tests and cell-culture; D.Q.

developed the resistance test-chip; J.Y. fabricated patterns using stereolithography; P.D. and S.S. performed FTIR experiments and imaging; P.S. conceived and designed the experiments. All authors contributed in writing the manuscript.

Acknowledgement

We acknowledge Syracuse Biomaterial Institute for providing equipment used for all the experiments in this paper. We thank Professor J. Henderson, Department of Biomedical and Chemical Engineering, Syracuse University, for donating 10T1/2 cells, Ciba Specialty Chemicals for donating Irgacure photoinitiator; Syracuse confocal facility, and Professor J. Gilbert, Department of Biomedical and Chemical Engineering, Syracuse University for training and access to EIS and SEM.

Appendix A. Supplementary data

Supplementary data associated with this article can be found, in the online version, at http://dx.doi.org/10.1016/j.actbio.2016.01.036.

References

[1] S. Yang, K.-F. Leong, Z. Du, C.-K. Chua, The design of scaffolds for use in tissue engineering. Part I. Traditional factors, Tissue Eng. 7 (2001) 679–689.
[2] L.G. Griffith, Emerging design principles in biomaterials and scaffolds for tissue engineering, Ann. N. Y. Acad. Sci. 961 (2002) 83–95.
[3] I. Smith, X. Liu, L. Smith, P. Ma, Nanostructured polymer scaffolds for tissue engineering and regenerative medicine, Wiley Interdiscip. Rev. Nanomed. Nanobiotechnol. 1 (2009) 226–236.
[4] S.J. Hollister, Porous scaffold design for tissue engineering, Nat. Mater. 4 (2005) 518–524.
[5] Q.L. Loh, C. Choong, Three-dimensional scaffolds for tissue engineering applications: Role of porosity and pore size, Tissue Eng. Part B: Rev. 19 (2013) 485–502.
[6] R. Langer, J.P. Vacanti, Tissue engineering, Science 260 (1993) 920–926.
[7] D.E. Ingber, V.C. Mow, D. Butler, L. Niklason, J. Huard, J. Mao, et al., Tissue engineering and developmental biology: going biomimetic, Tissue Eng. 12 (2006) 3265–3283.
[8] A.M. Kloxin, M.W. Tibbitt, K.S. Anseth, Synthesis of photodegradable hydrogels as dynamically tunable cell culture platforms, Nat. Protoc. 5 (2010) 1867–1887.
[9] K.J.R. Lewis, K.S. Anseth, Hydrogel scaffolds to study cell biology in four dimensions, MRS Bull. 38 (2013) 260–268.
[10] M.W. Tibbitt, K.S. Anseth, Hydrogels as extracellular matrix mimics for 3D cell culture, Biotechnol. Bioeng. 103 (2009) 655–663.
[11] K. Lee, D. Mooney, Hydrogels for tissue engineering, Chem. Rev. 101 (2001) 1869–1879.
[12] M. Lutolf, J. Hubbell, Synthetic biomaterials as instructive extracellular microenvironments for morphogenesis in tissue engineering, Nat. Biotechnol. 23 (2005) 47–55.
[13] N. Annabi, A. Tamayol, J.A. Uquillas, M. Akbari, L.E. Bertassoni, C. Cha, et al., 25th Anniversary Article: rational design and applications of hydrogels in regenerative medicine, Adv. Mater. 26 (2014) 85–124.
[14] C.A. DeForest, K.S. Anseth, Advances in bioactive hydrogels to probe and direct cell fate, Ann. Rev. Chem. Biomol. Eng. 3 (2012) 421–444.
[15] S. Sun, I. Titushkin, M. Cho, Regulation of mesenchymal stem cell adhesion and orientation in 3D collagen scaffold by electrical stimulus, Bioelectrochemistry 69 (2006) 133–141.
[16] E. Wang, M. Zhao, J.V. Forrester, C.D. McCaig, Re-orientation and faster, directed migration of lens epithelial cells in a physiological electric field, Exp. Eye Res. 71 (2000) 91–98.
[17] K.E. Hammerick, M.T. Longaker, F.B. Prinz, In vitro effects of direct current electric fields on adipose-derived stromal cells, Biochem. Biophys. Res. Commun. 397 (2010) 12–17.
[18] H.T.H. Au, I. Cheng, M.F. Chowdhury, M. Radisic, Interactive effects of surface topography and pulsatile electrical field stimulation on orientation and elongation of fibroblasts and cardiomyocytes, Biomaterials 28 (2007) 4277–4293.
[19] A.S. Rowlands, J.J. Cooper-White, Directing phenotype of vascular smooth muscle cells using electrically stimulated conducting polymer, Biomaterials 29 (2008) 4510–4520.
[20] S. Sundelacruz, M. Levin, D.L. Kaplan, Membrane potential controls adipogenic and osteogenic differentiation of mesenchymal stem cells, PLoS One 3 (2008) e3737.
[21] A. Guiseppi-Elie, Electroconductive hydrogels: synthesis, characterization and biomedical applications, Biomaterials 31 (2010) 2701–2716.
[22] F. Lamberti, S. Giulitti, M. Giomo, N. Elvassore, Biosensing with electroconductive biomimetic soft materials, J. Mater. Chem. B 1 (2013) 5083–5091.
[23] I. Rajzer, M. Rom, E. Menaszek, P. Pasierb, Conductive PANI patterns on electrospun PCL/gelatin scaffolds modified with bioactive particles for bone tissue engineering, Mater. Lett. 138 (2015) 60–63.
[24] R. Balint, N.J. Cassidy, S.H. Cartmell, Conductive polymers: towards a smart biomaterial for tissue engineering, Acta Biomater. 10 (2014) 2341–2353.
[25] J. Huang, X. Hu, L. Lu, Z. Ye, Q. Zhang, Z. Luo, Electrical regulation of Schwann cells using conductive polypyrrole/chitosan polymers, J. Biomed. Mater. Res., Part A 93 (2010) 164–174.
[26] L. Ghasemi-Mobarakeh, M.P. Prabhakaran, M. Morshed, M.H. Nasr-Esfahani, S. Ramakrishna, Electrical stimulation of nerve cells using conductive nanofibrous scaffolds for nerve tissue engineering, Tissue Eng. Part A 15 (2009) 3605–3619.
[27] M. Radisic, H. Park, H. Shing, T. Consi, F.J. Schoen, R. Langer, et al., Functional assembly of engineered myocardium by electrical stimulation of cardiac myocytes cultured on scaffolds, Proc. Natl. Acad. Sci. U.S.A. 101 (2004) 18129–18134.
[28] J.O. You, M. Rafat, G.J. Ye, D.T. Auguste, Nanoengineering the heart: conductive scaffolds enhance connexin 43 expression, Nano Lett. (2011).
[29] R.A. Green, N.H. Lovell, G.G. Wallace, L.A. Poole-Warren, Conducting polymers for neural interfaces: challenges in developing an effective long-term implant, Biomaterials 29 (2008) 3393–3399.
[30] R. Balint, N.J. Cassidy, S.H. Cartmell, Electrical stimulation: a novel tool for tissue engineering, Tissue Eng. Part B: Rev. 19 (2012) 48–57.
[31] C.J. Small, C.O. Too, G.G. Wallace, Responsive conducting polymer-hydrogel composites, Polym. Gels Networks 5 (1997) 251–265.
[32] T. Dvir, B.P. Timko, M.D. Brigham, S.R. Naik, S.S. Karajanagi, O. Levy, et al., Nanowired three-dimensional cardiac patches, Nat. Nanotechnol. 6 (2011) 720–725.
[33] S. Ahadian, R.B. Sadeghian, S. Yaginuma, J. Ramón-Azcón, Y. Nashimoto, X. Liang, et al., Hydrogels containing metallic glass sub-micron wires for regulating skeletal muscle cell behaviour, Biomater. Sci. 3 (2015) 1449–1458.
[34] K. Liu, Y. Li, F. Xu, Y. Zuo, L. Zhang, H. Wang, et al., Graphite/poly (vinyl alcohol) hydrogel composite as porous ringy skirt for artificial cornea, Mater. Sci. Eng., C 29 (2009) 261–266.
[35] S. Sayyar, E. Murray, B.C. Thompson, J. Chung, D.L. Officer, S. Gambhir, et al., Processable conducting graphene/chitosan hydrogels for tissue engineering, J. Mater. Chem. B 3 (2015) 481–490.
[36] C.J. Ferris, Conducting bio-materials based on gellan gum hydrogels, Soft Matter 5 (2009) 3430–3437.
[37] A.K. Gaharwar, N.A. Peppas, A. Khademhosseini, Nanocomposite hydrogels for biomedical applications, Biotechnol. Bioeng. 111 (2014) 441–453.
[38] R.A. MacDonald, C.M. Voge, M. Kariolis, J.P. Stegemann, Carbon nanotubes increase the electrical conductivity of fibroblast-seeded collagen hydrogels, Acta Biomater. 4 (2008) 1583–1592.
[39] S. Ahadian, J. Ramón-Azcón, M. Estili, X. Liang, S. Ostrovidov, H. Shiku, et al., Hybrid hydrogels containing vertically aligned carbon nanotubes with anisotropic electrical conductivity for muscle myofiber fabrication, Sci. Rep. (2014) 4.
[40] S.R. Shin, S.M. Jung, M. Zalabany, K. Kim, P. Zorlutuna, Kim. Sb, et al., Carbon-nanotube-embedded hydrogel sheets for engineering cardiac constructs and bioactuators, ACS Nano 7 (2013) 2369–2380.
[41] R.A. Green, R.T. Hassarati, J.A. Goding, S. Baek, N.H. Lovell, P.J. Martens, et al., Conductive hydrogels: mechanically robust hybrids for use as biomaterials, Macromol. Biosci. 12 (2012) 494–501.
[42] D. Mawad, E. Stewart, D.L. Officer, T. Romeo, P. Wagner, K. Wagner, et al., A single component conducting polymer hydrogel as a scaffold for tissue engineering, Adv. Funct. Mater. 22 (2012) 2692–2699.
[43] D.G. Harman, R. Gorkin, L. Stevens, B. Thompson, K. Wagner, B. Weng, et al., Poly (3,4-ethylenedioxythiophene): dextran sulfate (PEDOT: DS)–a highly processable conductive organic biopolymer, Acta Biomater. 14 (2015) 33–42.
[44] H. Ding, M. Zhong, Y.J. Kim, P. Pholpabu, A. Balasubramanian, C.M. Hui, et al., Biologically derived soft conducting hydrogels using heparin-doped polymer networks, ACS Nano 8 (2014) 4348–4357.
[45] E. Kang, K. Neoh, K. Tan, Polyaniline: a polymer with many interesting intrinsic redox states, Prog. Polym. Sci. 23 (1998) 277–324.
[46] P.R. Bidez, S. Li, A.G. MacDiarmid, E.C. Venancio, Y. Wei, P.I. Lelkes, Polyaniline, an electroactive polymer, supports adhesion and proliferation of cardiac myoblasts, J. Biomater. Sci. Polym. Ed. 17 (2006) 199–212.
[47] P. Humpolicek, V. Kasparkova, P. Saha, J. Stejskal, Biocompatibility of polyaniline, Synth. Met. 162 (2012) 722–727.
[48] Y. Guo, M. Li, A. Mylonakis, J. Han, A.G. MacDiarmid, X. Chen, et al., Electroactive oligoaniline-containing self-assembled monolayers for tissue engineering applications, Biomacromolecules 8 (2007) 3025–3034.
[49] L.M. Lira, S.I.C. de Torresi, Conducting polymer–hydrogel composites for electrochemical release devices: synthesis and characterization of semi-interpenetrating polyaniline–polyacrylamide networks, Electrochem. Commun. 7 (2005) 717–723.
[50] S.K. Siddhanta, R. Gangopadhyay, Conducting polymer gel: formation of a novel semi-IPN from polyaniline and crosslinked poly(2-acrylamido-2-methyl propanesulphonicacid), Polymer 46 (2005) 2993–3000.
[51] L.A. Samuelson, A. Anagnostopoulos, K.S. Alva, J. Kumar, S.K. Tripathy, Biologically derived conducting and water soluble polyaniline, Macromolecules 31 (1998) 4376–4378.

[52] Y. Cao, P. Smith, A. Heeger, Spectroscopic studies of polyaniline in solution and in spin-cast films, Synth. Met. 32 (1989) 263–281.
[53] L. Zhang, M. Wan, Self-assembly of polyaniline—from nanotubes to hollow microspheres, Adv. Funct. Mater. 13 (2003) 815–820.
[54] M. Li, Y. Guo, Y. Wei, A.G. MacDiarmid, P.I. Lelkes, Electrospinning polyaniline-contained gelatin nanofibers for tissue engineering applications, Biomaterials 27 (2006) 2705–2715.
[55] J. Cheung, M. Rubner, Fabrication of electrically conductive Langmuir–Blodgett multilayer films of polyaniline, Thin Solid Films 244 (1994) 990–994.
[56] J. Jang, J. Ha, J. Cho, Fabrication of water-dispersible polyaniline-poly(4-styrenesulfonate) nanoparticles for inkjet-printed chemical-sensor applications, Adv. Mater. 19 (2007) 1772–1775.
[57] O. Ngamna, A. Morrin, A.J. Killard, S.E. Moulton, M.R. Smyth, G.G. Wallace, Inkjet printable polyaniline nanoformulations, Langmuir 23 (2007) 8569–8574.
[58] Y. Wu, Y.X. Chen, J. Yan, S. Yang, P. Dong, P. Soman, Fabrication of conductive polyaniline hydrogel using porogen leaching and projection microstereolithography, J. Mater. Chem. B 3 (2015) 5352–5360.
[59] J.W. Nichol, S.T. Koshy, H. Bae, C.M. Hwang, S. Yamanlar, A. Khademhosseini, Cell-laden microengineered gelatin methacrylate hydrogels, Biomaterials 31 (2010) 5536–5544.
[60] P. Soman, P.H. Chung, A.P. Zhang, S. Chen, Digital microfabrication of user-defined 3D microstructures in cell-laden hydrogels, Biotechnol. Bioeng. 110 (2013) 3038–3047.
[61] J. Ramón-Azcón, S. Ahadian, R. Obregón, G. Camci-Unal, S. Ostrovidov, V. Hosseini, et al., Gelatin methacrylate as a promising hydrogel for 3D microscale organization and proliferation of dielectrophoretically patterned cells, Lab Chip 12 (2012) 2959–2969.
[62] K. Yue, G. Trujillo-de Santiago, M.M. Alvarez, A. Tamayol, N. Annabi, A. Khademhosseini, Synthesis, properties, and biomedical applications of gelatin methacryloyl (GelMA) hydrogels, Biomaterials 73 (2015) 254–271.
[63] V. Guarino, M.A. Alvarez-Perez, A. Borriello, T. Napolitano, L. Ambrosio, Conductive PANi/PEGDA macroporous hydrogels for nerve regeneration, Adv. Healthcare Mater. 2 (2013) 218–227.
[64] T. Dai, X. Qing, J. Wang, C. Shen, Y. Lu, Interfacial polymerization to high-quality polyacrylamide/polyaniline composite hydrogels, Compos. Sci. Technol. 70 (2010) 498–503.
[65] J. Huang, R.B. Kaner, A general chemical route to polyaniline nanofibers, J. Am. Chem. Soc. 126 (2004) 851–855.
[66] D.D. Sawall, R.M. Villahermosa, R.A. Lipeles, A.R. Hopkins, Interfacial polymerization of polyaniline nanofibers grafted to Au surfaces, Chem. Mater. 16 (2004) 1606–1608.
[67] M.R. Abidian, D.H. Kim, D.C. Martin, Conducting-polymer nanotubes for controlled drug release, Adv. Mater. 18 (2006) 405–409.
[68] C. Dispenza, C.L. Presti, C. Belfiore, G. Spadaro, S. Piazza, Electrically conductive hydrogel composites made of polyaniline nanoparticles and poly(N-vinyl-2-pyrrolidone), Polymer 47 (2006) 961–971.